3-D Interferometric optoacoustic imaging

Stefan A. Carp[a,c], and Vasan Venugopalan[a,b,c]

[a]Department of Chemical Engineering and Materials Science, University of California – Irvine, Irvine, CA 92697;
[b]Department of Biomedical Engineering, University of California – Irvine, Irvine, CA 92697;
[c]Laser Microbeam and Medical Program, Beckman Laser Institute, 1002 Health Sciences Road East, Irvine, CA 92612

ABSTRACT

We report on the further development of our previously described spectroscopic imaging technique based on time-resolved interferometric measurements of laser-induced thermoelastic expansion (POISe: Pulsed Optoelastic Interferometric Spectroscopy and Imaging). We show the capability of POISe to form tomographic images of tissue phantoms and live animal tissues. By performing image reconstruction on data sets acquired from several tissue-like phantoms we demonstrate the ability of POISe to provide better than 200 μm spatial resolution in a strongly scattering medium (μ_s'=1.5/mm). Additionally we demonstrate the ability of POISe to image chicken chorio-allantoic membrane (CAM) blood vessels through a 6–10 mm layer of Intralipid with μ_s'=0.75/mm.

Keywords: photoacoustic, interferometer, beam forming, image reconstruction, thermoelastic effect

1. INTRODUCTION

Optoacoustic methods have emerged over the past decade as a medical technology capable of imaging tissue structures with submillimeter resolution up to several centimeters in depth. These capabilities have been demonstrated in tissue phantoms,[1–8] *in-vitro*[9,10] and *in-vivo*.[11,12] By using pulsed laser irradiation to excite acoustic waves and then detecting the arrival of these acoustic waves at the tissue surface using a variety of methods optoacoustic imaging combines the deep penetration of red/near-infrared light with endogenous/exogenous optical contrast and the relatively non-dispersive propagation of ultrasonic waves to provide images with sub-millimiter resolution.

Here we describe the further development of a novel optoacoustic technique termed POISe (Pulsed Optoacoustic Interferometric Spectroscopic Imaging) for imaging and physiological characterization of heterogeneous tissues at depths approaching 1 cm with a spatial resolution better than μm.[8] In contrast to optoacoustic implementations based on the detection of stress transients, POISe measures the surface displacement of a tissue sample resulting from pulsed laser irradiation. The advantages of our approach are its non-contact nature which eliminates the need for acoustic coupling between the sample and the detection system as well as the potential for increased lateral resolution stemming from the ability to focus the interferometer probe beam to a diffraction limited size.

2. MATERIALS AND METHODS

2.1. Experimental Setup

Figure 1 is a schematic of the current POISe system. This system has been described previously.[8,13,14] Briefly, a pulsed pump laser beam irradiates the sample, generating the thermal expansion that is measured by a modified Mach-Zehnder interferometer in conjunction with associated electronics and a computer control system. The interferometer employs a polarized He-Ne laser (λ=632.8 nm), whose output is split by an acousto-optic modulator (ATM-1101A1, IntraAction) driven at 110 MHz. A portion of the He-Ne beam travels undisturbed through the AOM, while the rest is deflected into several frequency shifted beams. One of the first order frequency

Send correspondence to Vasan Venugopalan
E-mail: vvenugop@uci.edu, Telephone: 1 949 824 5802, Fax: 1 949 824 2541

Photons Plus Ultrasound: Imaging and Sensing 2005, edited by Alexander A. Oraevsky, Lihong V. Wang, Proceedings of SPIE Vol. 5697 (SPIE, Bellingham, WA, 2005)
1605-7422/05/$15 · doi: 10.1117/12.591134

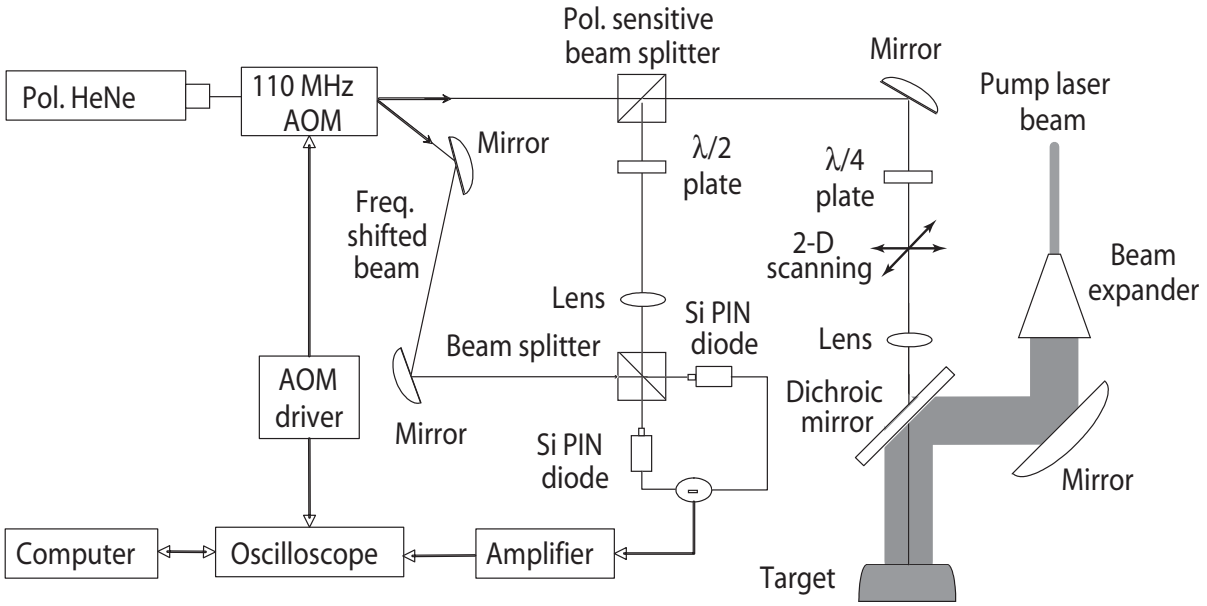

Figure 1. Schematic of the current POISe system. A Q-switched Nd:YAG laser operating at 532/1064 nm irradiates the sample, generating thermal expansion which is measured with an interferometric system employing a modified Mach Zehnder interferometer.

shifted beams ($\Delta f = 110$ MHz) is picked off by a mirror and forms the reference arm of the interferometer. The unshifted beam enters the sample arm of the interferometer, eventually reflecting off the sample surface. The polarization optics redirect the returning sample beam for recombination with the reference beam at the 50/50 beamsplitter. The beams emerging from the beamsplitter are directed to two Si PIN photodiodes (Hamamatsu). The signal is further amplified using a broadband low-noise amplifier (Mini-Circuits) and digitized by a 500 MHz bandwidth digital oscilloscope (Tektronix).

2.2. Imaging targets

The POISe system has been demonstrated to achieve 200μm lateral resolution in two-dimensional image reconstructions performed on tissue-like phantoms.[8] To examine the ability of POISe to form *three-dimensional* tomographic images of heterogeneous structures two test systems were used: tissue-like phantoms and a simple animal model.

2.2.1. Tissue-like phantoms

Phantoms were built to simulate a pair of blood vessels immersed in a turbid tissue. The optical properties were targeted to mimic those of a typical tissue in the near-infrared. The scattering medium was a 2% Intralipid solution possessing a reduced scattering coefficient of μ_s'=1.5 mm^{-1}. Simulated vessels were fashioned using thin hollow polyimide tubes (Cole-Parmer) with an outer diameter of 160 μm and an internal diameter of 120 μm through which a dilute solution of India ink with μ_a=0.5 mm^{-1} was circulated to simulate the absorption of whole blood at λ=1064 nm. A Q-switched Nd:YAG laser (Quantel) operating at λ=1064 nm with a 5 ns pulse duration and 22.5 mm beam diameter (after expansion) was used as the pump laser beam with an incident radiant exposure of 110 mJ/cm^2. At this wavelength the polyimide tubes are essentially transparent, and their contribution to the displacement signal is negligible.

2.2.2. Animal model

The chicken chorio-allantoic membrane (CAM) vasculature was chosen as an *in-vivo* animal model. Fertilized chicken eggs 3.5 days old were opened and their contents transferred into transparent plastic cups which were

then covered with a breathable film and incubated at 38 ° C for an additional 5 days. At day 9, the CAM was almost fully developed, presenting a surface covered with a vascular network. For the purpose of our experiments a 0.5% Intralipid solution (μ_s'=0.75/mm at 532 nm) was poured on top of the membrane to a thickness of 6–10 mm. A Q-switched Nd:YAG laser (Quantel) operating at λ=532 nm with a 5 ns pulse duration and 18 mm beam diameter (after expansion) was used to irradiate the sample with an incident radiant exposure of 80 mJ/cm^2.

2.3. Image reconstruction principles

We employed a simple delay and sum beam-forming algorithm to reconstruct images from multiple surface displacement measurements acquired at distinct locatinns.[2] The tissue volume was divided into small volume elements (voxels) and each of them was evaluated as a potential source from which a thermoelastic disturbance can emanate and be detected by measurements taken at different locations on the tissue surface. The delay and sum method determines the acoustic source intensity for each voxel by finding the time window within each time-resolved surface displacement trace that corresponds to the interior of the current voxel and performing a weighted sum of the averaged displacement signals in that window for all the detectors,

$$I(\boldsymbol{r}) = \frac{\sum_i w_i^d \left\langle S_i \left[\frac{(\boldsymbol{r}_i^d - \boldsymbol{r}) - l/2}{c_a} : \frac{(\boldsymbol{r}_i^d - \boldsymbol{r}) + l/2}{c_a} \right] \right\rangle}{\sum_i w_i^d} \tag{1}$$

where $\boldsymbol{r}$ is the location in the imaged volume, $I(\boldsymbol{r})$ is the acoustic source intensity corresponding to location $\boldsymbol{r}$, $\sum_i$ denotes a sum over all the detection points, w_i^d is a detector specific weighting factor, $S_i(t)$ is the time-resolved signal from the ith detector, $\boldsymbol{r}_i^d$ is the location of the ith detector, c_a is the speed of sound and l is the voxel size, : denotes the set of discrete displacements acquired within the time window of interest, and $<\ >$ denotes averaging the signal over the time interval corresponding to the transit time across the voxel in question. The set of weights w_i^d can be used to improve different characteristics of the formed image by compensating, for example, for the effects of geometrical attenuation or acoustic absorption as the signal travels from the focus point to the individual detectors.

3. RESULTS AND DISCUSSION

3.1. Preliminary three-dimensional image reconstructions

Figure 2 shows a photograph of a tissue-like phantom in which two 120 μm internal diameter polyimide tubes were suspended on a plastic support and crossed at an approximately 45° angle. The support was placed in a container which was filled with Intralipid (as described previously) until the tubes were approximately 4 mm below the Intralipid surface. Surface displacement measurements were taken within a 10 × 32 mm rectangular area at locations spaced at 1 × 0.5 mm increments. This provided a 65x11 array of measurement locations. Figure 3 shows the "top-view" of a three-dimensional reconstruction of a 4 × 10 × 10 mm volume roughly centered over the intersection point of the tubes using the Maximum Intensity Projection (MIP) method.[15] The quality of the reconstructed image is very good, matching the actual geometry of the phantom well. The diameter of the tubes is less than 200 μm, in keeping with the demonstrated 200 μm lateral resolution of our method.[8]

Figure 3 shows a photograph of the CAM target, with blood vessels clearly visible on the surface. Intralipid was added on top of the CAM as described previously, followed by the acquisition of surface displacement traces on a 10 × 30 mm rectangular area spaced 1 mm apart. This provided a 31x11 array of measurement locations. Figure 4 shows the MIP "top-view" of a three-dimensional reconstruction of a 24 × 10 × 20 mm volume indicate by a rectangle in Figure 3 together with the matching, zoomed-in region of the photograph in Figure 3. Several blood vessels are visible with branching points and inter-vessel angles matching the photograph of the CAM very well.

These images show the capability of POISe to form high-resolution three-dimensional images of *in-vitro* and *in-vivo* structures at significant depths.

ACKNOWLEDGMENTS

We acknowledge support from the NIH through the Laser Microbeam and Medical Program (P41-RR-01192)

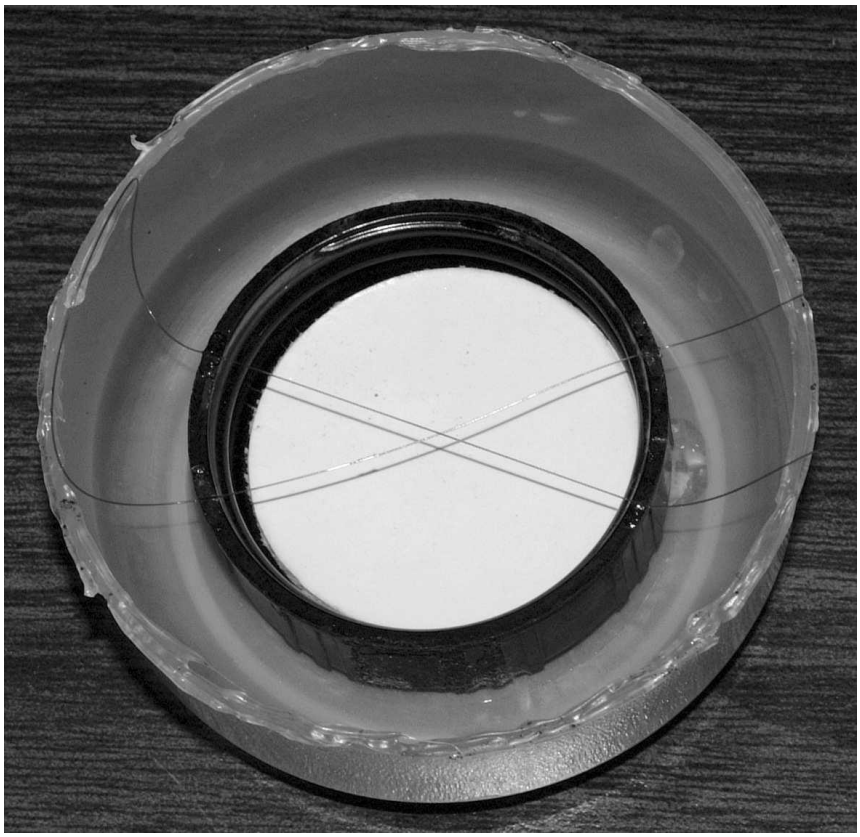

Figure 2. Photograph of the polyimide tube phantom before Intralipid was added.

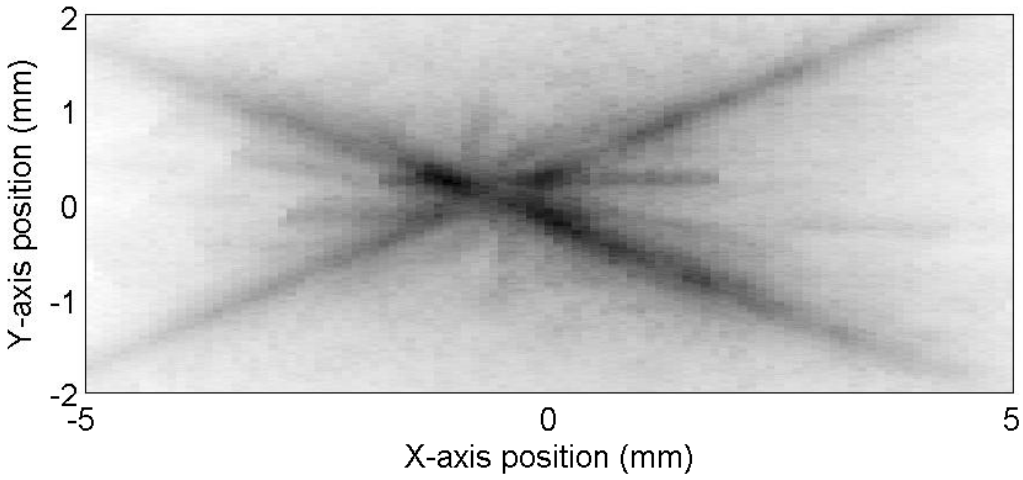

Figure 3. Maximum intensity projection top-view reconstruction of the polyimide tube phantom.

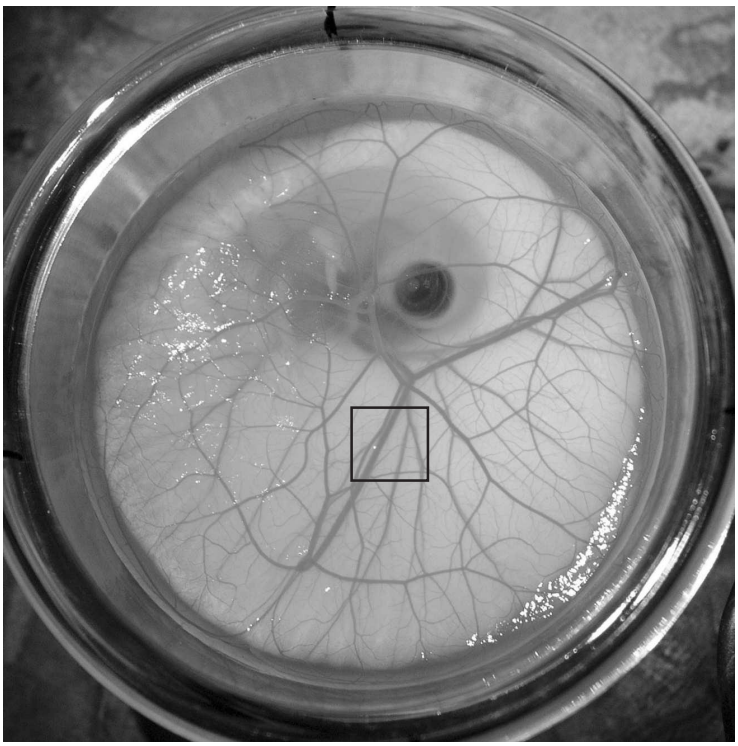

Figure 4. Photograph of the CAM membrane before Intralipid was added. Square indicates the image reconstruction area.

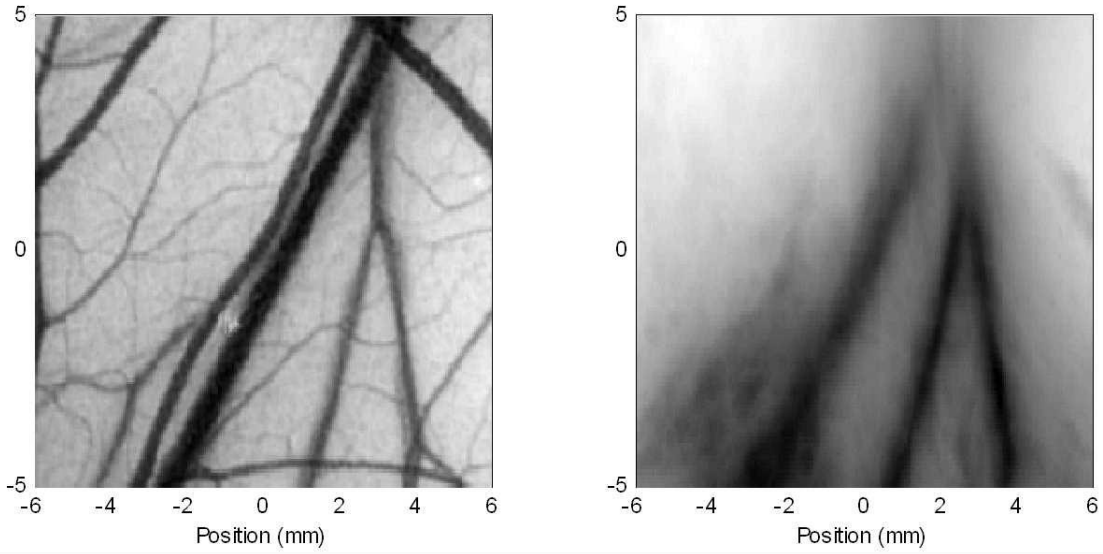

Figure 5. Photograph and maximum intensity projection top-view reconstruction of the CAM blood vessels.

REFERENCES

1. R. Kruger, P. Liu, Y. Fang, and C. R. Appledorn, "Photoacoustic ultrasound (PAUS)–reconstruction tomography," *Med. Phys.* **22**(10), pp. 1605–1609, 1995.
2. C. G. A. Hoelen and F. F. M. de Mul, "Image reconstruction for photoacoustic scanning of tissue structures," *Appl. Optics* **39**(31), pp. 5872–5883, 2000.
3. K. P. Kostli, M. Frenz, H. P. Weber, G. Paltauf, and H. Schmidt-Kloiber, "Optoacoustic tomography: time-gated measurement of pressure distributions and image reconstruction," *Appl. Optics* **40**(22), pp. 3800–3809, 2001.
4. X. D. Wang, Y. Xu, M. H. Xu, S. Yokoo, E. S. Fry, and L. H. V. Wang, "Photoacoustic tomography of biological tissues with high cross-section resolution: Reconstruction and experiment," *Medical Physics* **29**(12), pp. 2799–2805, 2002.
5. K. P. Kostli and P. C. Beard, "Two-dimensional photoacoustic imaging by use of fourier-transform image reconstruction and a detector with an anisotropic response," *Appl. Optics* **42**(10), pp. 1899–1908, 2003.
6. G. Paltauf, H. Schmidt-Kloiber, K. P. Kostli, and M. Frenz, "Optical method for two-dimensional ultrasonic detection," *Appl. Phys. Lett.* **75**(8), pp. 1048–1050, 1999.
7. J. J. Niederhauser, D. Frauchiger, H. P. Weber, and M. Frenz, "Real-time optoacoustic imaging using a schlieren transducer," *Appl. Phys. Lett.* **81**(4), pp. 571–573, 2002.
8. S. A. Carp, A. Guerra, S. Q. Duque, and V. Venugopalan, "Optoacoustic imaging using interferometric measurement of surface displacement," *Appl. Phys. Lett.* **85**(23), pp. 5772–5774, 2004.
9. M. C. Pilatou, N. J. Voogd, F. F. M. de Mul, L. N. A. van Aldrichem, and W. Steenbergen, "Analysis of three-dimensional photoacoustic imaging of a vascular tree *in vitro*," *Rev. Sci. Instr.* **74**(10), pp. 4495–4499, 2003.
10. R. A. Kruger, W. L. Kiser, D. Reinecke, G. A. Kruger, and K. D. Miller, "Thermoacoustic molecular imaging of small animals," *Molecular Imaging* **2**, pp. 113–123, April 2003.
11. A. A. Karabutov, E. V. Savateeva, and A. A. Oraevsky, "Optoacoustic tomography: New modality of laser diagnostic systems," *Laser Phys.* **13**(5), pp. 711–723, 2003.
12. X. D. Wang, Y. J. Pang, G. Ku, X. Y. Xie, G. Stoica, and L. H. V. Wang, "Noninvasive laser-induced photoacoustic tomography for structural and functional in vivo imaging of the brain," *Nat. Biotech.* **21**(7), pp. 803–806, 2003.
13. B. P. Payne, V. Venugopalan, B. B. Mikić, and N. S. Nishioka, "Optoacoustic determination of optical attenuation depth using interferometric detection," *J. Biomed. Opt.* **8**(2), pp. 264–272, 2003.
14. B. P. Payne, V. Venugopalan, B. B. Mikić, and N. S. Nishioka, "Optoacoustic tomography interferometric detection using time-resolved of surface displacement," *J. Biomed. Opt.* **8**(2), pp. 273–280, 2003.
15. P. S. Calhoun, B. S. Kuszyk, D. G. Heath, J. C. Carley, and E. K. Fishman, "Three-dimensional Volume Rendering of Spiral CT Data: Theory and Method," *Radiographics* **19**(3), pp. 745–764, 1999.